



## Assessment of Heavy Rainfall using GPM- IMERG Satellite Product over Nepal

Nirmala Regmi<sup>1, 2 \*</sup>, Bikash Nepal<sup>2</sup>, Shankar Sharma<sup>1</sup>, Dibas Shrestha<sup>1</sup> and Govind Kumar Jha<sup>2</sup>

<sup>1</sup> Central Department of Hydrology and Meteorology (CDHM), Kirtipur, Kathmandu, Nepal

<sup>2</sup> Department of Hydrology and Meteorology (DHM), Government of Nepal, Kathmandu, Nepal

### ARTICLE INFO

Received: 20 August 2021

Received in Revised form: 6 October 2021

Accepted: 12 October 2021

Available Online: 2 December 2021

### Keywords

Satellite

IMERG

Extreme rainfall

Nepal

MODE

### \*Correspondance

Nirmala Regmi

nirmalaregmi52@gmail.com

**Abstract:** This study evaluates the Integrated Multi-satellite Retrievals from Global Precipitation Measurement (IMERG) final product's ability to represent the extreme precipitation against 310 observations from Nepal between 2015 and 2017. Additionally, Method of Object-based Diagnostic Evaluation (MODE) analysis was also performed to analyze IMERG ability to capture actual spatial distribution of the rainfall extremes. Both datasets show the extreme rainfall events are mostly concentrated at southern low land areas of the country. MODE tool further revealed the slight shifting of heavy precipitation location by IMERG product as compared to observation. It is also noted that, as precipitation intensity increases (threshold values of rainfall), the number of extreme events decreases. Moreover, this work provides a systematic quantification of the performance of IMERG gauge calibrated product and its applicability in extreme precipitation over mountainous region.

## 1. Introduction

Precipitation measurement is the primary input for different hydro-meteorological and climate models, which are used to predict different natural hazards such as floods, droughts and landslides (Li et al., 2013). Further, accurate estimation of precipitation is very important for development, calibration and validation of hydrological models (Sharifi et al., 2018). However, measuring accurate precipitation is always a challenging task for all meteorological authorities and scientists because of its discrete nature in both space and time (Nepal et al., 2021).

There are various methods of precipitation measurement. Among them, the rain gauge (i.e., point measurements) measurements are the most widely used techniques for precipitation estimation (Qiaohong et al., 2017). Rain gauges provide a direct measurement of precipitation, however, data collected from gauges may be subject to many potential operational errors such as instrumental and measurement error related to rain type (heavy rainfall) or associated with an external factor such as wind and evaporation and the distribution of gauges especially in mountainous regions (Hamal et al., 2020a; Hamal et al., 2020b; Sharma et al., 2020a). The use of ground-based weather radar enables the monitor and measurement of rainfall over relatively large areas in near real time; however, radar measurement suffers from error characteristics such as random error, obstruction by topography, range dependent systematic errors (Germann et al., 2007). Besides these limitations, radar systems are too expensive and difficult to maintain, thus, are not a feasible option for least developed as well as most of developing countries (Coning, 2013). Hence, freely available satellite precipitation products (SPPs) with quasi-global coverage are potential alternatives for precipitation measurement, especially for the data-sparse region (Soo et al., 2020).

In the recent years, several satellite-based precipitation products have been developed and applied in various hydro-meteorological applications globally. Satellite precipitation products (SPPs) are emerging as a potential measurement approach in recent decades (Tan et al., 2015; Xu et al., 2017). Recently developed SPPs and their use in various hydro-meteorological applications has drawn much attention towards their reliability (Sunilkumar et al., 2019). Several studies have been conducted on evaluating SPPs reliability across the globe. Sunilkumar et al., (2019) compared the IMERG product with gauge-based gridded precipitation products i.e. Asian Precipitation—Highly Resolved Observational Data Integration towards Evaluation (APHRODITE) over the Asian region and found that IMERG showed a good agreement with APHRODITE at different rainfall intensities, although it underestimated heavy precipitation events. Similarly, Tang et al., (2015) concluded that the IMERG has a very high correlation with ground-based measurements at the daily scale in China but only a moderate correlation in Iran (Sharifi et al., 2016) and the Blue Nile Basin (Sahlu et al., 2016). These studies found that in general the monthly and annual precipitation measurements of SPPs are more reliable than the daily precipitation measurement.

Moreover, areas having an insufficient gauge network and radar system, satellite-derived rainfall can be “a critical tool for identifying hazards from smaller-scale rainfall and flood events” (Coning, 2013). Since, SPPs are indirect measurements and suffer from various uncertainties and discrepancies, they should be evaluated and validated before operational use.

A recent study carried out by Sharma et al., (2020) found that IMERG products shows better performance on detecting precipitation events than TMPA. In addition, IMERG products show superior performances on daily time scales, while TMPA performs better at monthly time scale. Additionally, authors also mentioned that IMERG product can be a potential alternative to monitor extreme precipitation events and drought over Nepal. Furthermore, Nepal et al., (2021) revealed IMERGs better performance on capturing daily precipitation extremes (RX1Day and RX5Day) against GSMaP over Nepal's complex terrain.

Most of the above-mentioned studies (Nepal et al., 2021; Sharma et al., 2020a; Hamal et al., 2020a) were focused on evaluating SPPs performance based on various statistical skill scores and extreme precipitation indices. Karki et al., (2018) has also revealed about the spatial shifting of precipitation areas in IMERG estimates over Nepal for one single event and suggested for further study on this. Therefore, in this study an attempt is done to use MODE verification tool on assessing IMERGS ability to detect precipitation location focusing on extreme events over Nepal utilizing the large number (310) of observation station data as a reference. Traditional forecast verification techniques calculate skill scores based on point to point or grid to grid forecast-observation statistics. These approaches do not give any insight about the ways about the right or wrong forecast. Therefore, this cannot be used to find faults which can be helpful in improving the forecast. Method of Object-Based Diagnostic Evaluation (MODE) is new generation spatial verification method (Davis et al., 2009). These approaches permit an evaluation of forecast skill in more consistent way. Two fields can be compared using the MODE. Forecast can be referred as field one and observation can be referred as second field. Object attributes are calculated and compared, and are used to associate (merge) objects within a single field, as well as to match objects between the forecast and observed fields. The main goal of this research work is to evaluate the performance of IMERG product using large scale ground stations over Nepal and to examine the accuracy of the IMERG in estimating extreme events and detect the position of heavy rainfall events.

## **2. Materials and Methods**

### **2.1 Study Area**

Nepal is a mountainous country located on the southern slope of the central Himalayas (Figure 1) covering an area of 1, 47,516 km<sup>2</sup>. It is extended within an east-west distance of about 885 km and north-south distance of about 193 km from 26° 22' N to 30° 27' N in latitude to 80° 40' E to 88° 12' E in longitude. Rapid altitudinal gradient from 59 m in the southern Terai plane to Mount Everest 8,848.86 m in the northern Himalayan range leads to heterogeneous weather and climatic distribution over the country. South Asian Summer Monsoon (SASM) and westerlies dominate the seasonal variability with maximum rainfall during the summer monsoon season (June–September) with ~80% of annual precipitation followed by pre-monsoon (March–May, 12.5%), post-monsoon (October–November, 4.0%), and winter (December–February, 3.5%) (Karki et al., 2017; Nayava, 1980). Monsoon season is extensively wet with large amount of rainfall throughout the country. Nepal receives winter precipitation during the winter season in the form of snow in the high elevation areas. The annual cycle of

precipitation shows that July receives the highest precipitation followed by August, and it is equal to half of the total annual precipitation (Talchabhadel et al., 2018).

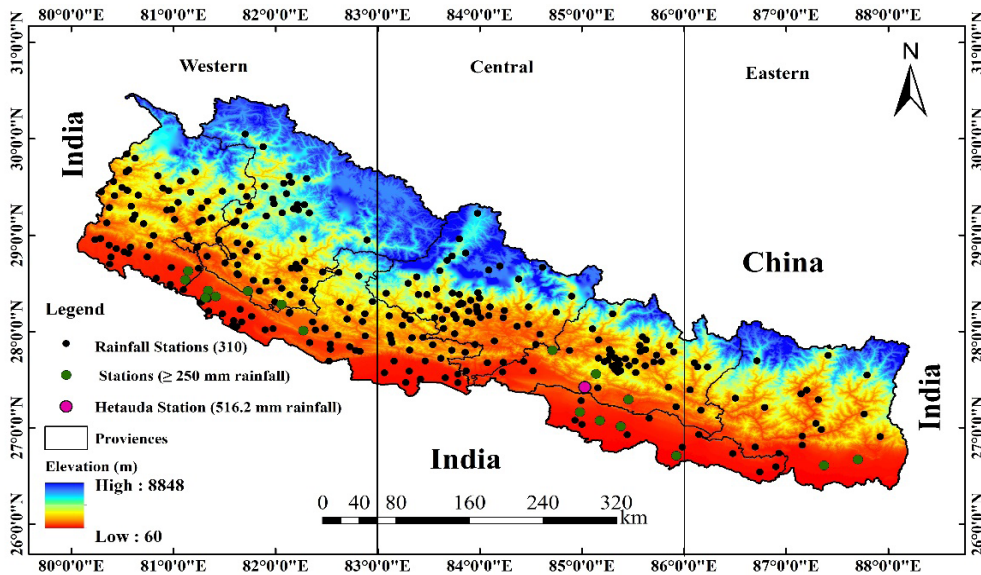


**Figure 1.** Study area and spatial distribution of selected 310 ground stations over the study region. The study area was divided into three subregions: Western (80-82°E), Central (83-85°E) and Eastern (86-88°E).

## 2.2 Data sets

### 2.2.1 Ground station data

For this study, the rainfall observations from 310 ground stations maintained by the Department of Hydrology and Meteorology (DHM), Nepal were used for the time period from December, 2015 to December, 2017 (Figure 1). Each 24 hour cumulative rainfall is measured at 03:00 UTC due to local time is 5 hour 45 minutes ahead of UTC time. This implies that a measurement dated 1st December includes the interval from 30th November 03:00 to 1st December 03:00 UTC.

### 2.2.2 IMERG product

In order to provide a finer and more accurate global precipitation estimation, NASA and JAXA have launched Global Precipitation Measurement (GPM) as the successor of TRMM in early 2014. Among different products of GPM, IMERG product with 0.1° spatial resolution and half an hour temporal resolution is used in this study. Depending on the calibration time, IMERG provides three types of products: the near-real-time “Early” run and “Late” run product, and the post-real-time “Final” run product. The IMERG “Early” run (hereafter called IMERG-E) and the “Late” run (hereafter called IMERG-L) product are released about 4 h and 12 h after the observation time respectively while the IMERG “Final” run (hereafter called IMERG-F) product is

released about 2.5 months after the observation. Early and Late run are multi-satellite precipitation product, while, Final run is calibrated with the Global Precipitation Climatology Centre (GPCC) precipitation gauge analysis (Hou et al., 2014; Huffman et al., 2019), and mostly recommended for research. The IMERG satellite constellation consists of one core observatory (GPM-CO) satellite and about ten partner satellites, equipped with the latest Dual-frequency Precipitation Radar (DPR), conical-scanning multichannel IMERG Microwave Imager (GMI) and many other advanced instruments, which can detect heavy to light rain and snow (Huffman et al., 2019). In this study, freely available IMERG L3 Day-1 IMERG Final Run V06 (IMERG\_3IMERGHH) (hereafter IMERG), data is used.

## 2.3 Methodology

### 2.3.1 Gridded data preparation

The daily data collected from DHM were made interpolated in R Studio using widely used interpolation technique, ordinary kriging. Kriging incorporates spatial correlation between stations and provides unbiased predictions with minimum variance (Li et al., 2013). Kriging has become a widely preferred interpolation method to estimate the spatial distribution of climate variables including rainfall (Adhikary et al., 2017). Therefore, in this study observed rainfall from stations were interpolated to  $0.1^\circ \times 0.1^\circ$  using ordinary kriging method to be used for assessment of IMERG at grid level.

### 2.3.2 Evaluation statistics

The continuous statistical metrics such as Standard Deviation (SD), Correlation Coefficient (CC), Root Mean Square Error (RMSE) and Relative Bias (RB) were used to quantitatively compare the performance of the Satellite Precipitation estimates relative to the precipitation gauges taken as the reference.

$$SD = \sqrt{\frac{\sum_{i=1}^n (R_i - \bar{R})^2}{(n-1)}} \quad (1)$$

$$CC = \frac{\sum_{i=1}^n (O_i - \bar{O})(S_i - \bar{S})}{\sqrt{\sum_{i=1}^n (O_i - \bar{O})^2} \sqrt{\sum_{i=1}^n (S_i - \bar{S})^2}} \quad (2)$$

$$RMSE = \sqrt{\frac{1}{n} \sum_{i=1}^n (S_i - O_i)^2} \quad (3)$$

$$RB = \frac{\sum_{i=1}^n (S_i - O_i)}{\sum_{i=1}^n S_i} * 100\% \quad (4)$$

Where,

- n=number of samples;
- R=mean precipitation;
- S<sub>i</sub>= i<sup>th</sup> value of satellite estimated rainfall;
- S = mean satellite estimated precipitation;
- O<sub>i</sub>= i<sup>th</sup> value of Gauged precipitation;
- o= Mean Gauged Precipitation

To evaluate the precipitation detection capability, we used following categorical statistical metrics:

**Accuracy:** Accuracy shows the overall percent correctness of the forecast. The value ranges from 0 to 1 and the perfect score is 1.

**Bias Score or Frequency Bias (BIAS):** The bias score or frequency bias (BIAS) is the ratio of the total events forecast to the total events observed. The forecast system is said to have a tendency to over-forecast or under-forecast events if BIAS>1 or BIAS<1 respectively.

**Probability of Detection (POD):** POD represents the ratio of precipitation occurrences correctly detected by the SPPs to the total number of actual precipitation events. The perfect score is 1 which represents the accurate detection (forecast).

**False Alarm Ratio (FAR):** FAR reveals the ratio of precipitation occurrences falsely detected to the total number of detected precipitation events. The perfect score for FAR is 0.

**Threat score (TS):** TS describes the overall ratio of precipitation events correctly detected by the SPPs. The value ranges from 0 to 1 with upper limit representing perfect score.

### 2.3.3 MODE verification

For this study, MODE is applied for manual observed data and IMERG. Firstly, all these precipitation data are regrided to regular lat/lon grid of 4 km using bilinear interpolation in NCAR Command Language (NCL). MODE analysis is carried out by considering manual observation as a reference. Precipitation objects are defined for threshold values 150/100 mm, 100/75mm, 75/50mm/24hr. for individual objects and cluster. Here in 150/100mm, 150mm denotes the 24 hour rainfall in a station and 100 mm denotes rainfall within defined cluster and similar definition for other two threshold values. This allows us to focus on very intense phenomena only, and to eliminate regions with little precipitation amounts that are not relevant in the context of this extreme precipitation study. For a particular object pair, the total interest (Davis et al., 2009) is defined as:

$$I_j = \frac{\sum_{i=1}^M c_i w_i F_{i,j}}{\sum_{i=1}^M c_i w_i} \quad (5)$$

Where, I<sub>j</sub> is the j-th objects pair and i indicates the number of the single evaluation attributes. M is the total number of attributes considered. F is the interest function which covers a scale from 0 to 1 and quantifies the agreement of the observed and modeled object characteristics.

### 3. Results

#### 3.1 Extreme Rainfall Event: A Case Study

Here in this study, one of the severe extreme rainfall events that occurred on 12-13 August, 2017 in the central and south-eastern parts of the country is investigated, which resulted floods in 21 districts in Terai belt (Disaster & Governments, 2017). The highest rainfall of 516.2 mm recorded on 13 August at Hetauda climate station, while 18 stations reported greater than 250 mm/day rainfall.

The performance of IMERG in estimating precipitation of that particular event, which occurred on 13 August, 2017 was investigated. The spatial distribution of observed rainfall shows the highest rainfall area around foothill of central Himalayan (Figure2). In addition, other two isolated rainfall areas around south-east Terai and western Terai are shown from spatial distribution of observed rainfall (Figure 2a). However, the spatial extent of the extreme precipitation estimated by IMERG shows that the IMERG captures the general pattern of extreme precipitation reasonably well with underestimation of rainfall amount. Further, the zone of maximum precipitation is spatially shifted towards west (Figure 2b). Also, the statistical verification of IMERG satellite product is carried out by calculating several statistical metrics.

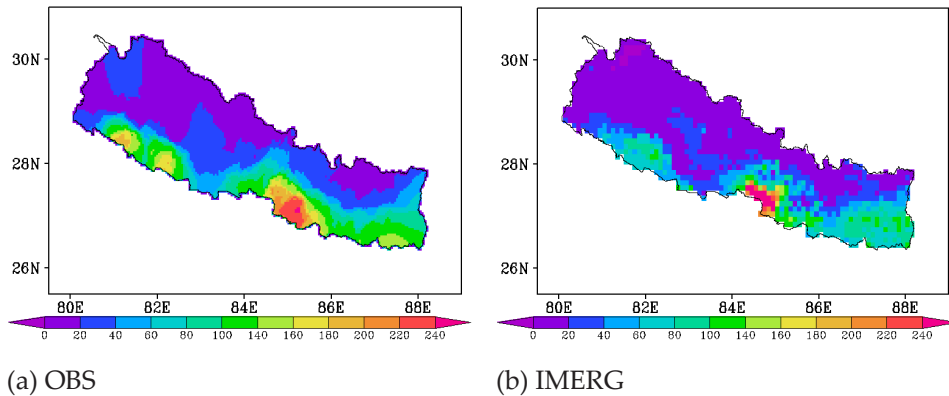


Figure 2. Spatial distribution of 1-day extreme rainfall on 13 August, 2017

Table 1. Categorical scores for extreme rainfall event

Threshold	Accuracy	POD	FAR	TS
$\geq 1\text{mm}$	0.96	1.00	0.05	0.95
$\geq 10$	0.78	0.84	0.15	0.73
$\geq 25$	0.77	0.81	0.27	0.62
$\geq 50$	0.82	0.74	0.34	0.53
$\geq 75$	0.80	0.50	0.65	0.26
$\geq 100$	0.84	0.44	0.85	0.12

**Table 2.** Summary for continuous statistical scores for extreme rainfall event

CC	SD	BIAS	RMSE
0.54	42.13	0.62	76.47

Statistical performance measures like Accuracy, POD, FAR, BIAS and TS were applied for each threshold across the whole country, by using a 2x2 contingency table. In this study, primarily higher thresholds of precipitation were focused since the devastating flood and landslide are consequences of high precipitation rates.

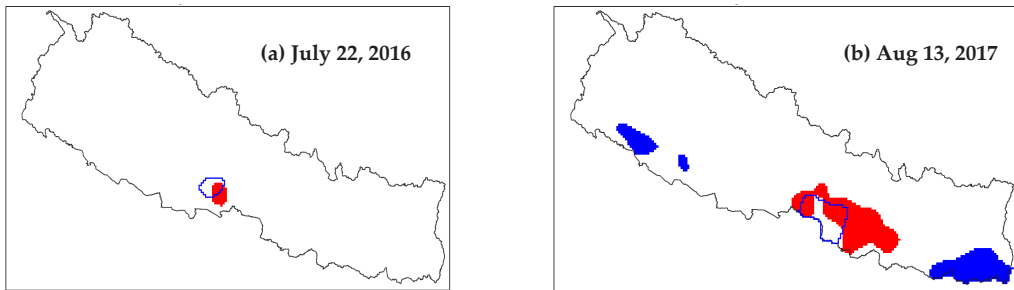
Table 1 indicates that the IMERG has good precipitation detection ability (POD) at lower threshold value. The detection capacity decreases with increasing threshold value. Higher accuracy and lower FAR for threshold value of  $\geq 1$ mm depicts the good estimation of rainy days. On increasing threshold values of rainfall, accuracy is simultaneously found to be increasing with threshold values which conclude that the IMERG gives comparatively accurate result for this particular event. Statistical metrics of the IMERG during the 2017 flood event is shown in Table 2.

### 3.2 MODE Object Based Verification

Following the MODE technique using NCAR MET tool, precipitation objects for SPPs and observation have been identified corresponding to different threshold value of 150/100, 100/75 and 75/50 mm/24 hr. (Figure 3, 4 and 5) for individual object and cluster. This process allows us to focus only on intense phenomenon by filtering out lighter rain areas which are not meaningful for this study. The extreme events are selected based on having rainfall equal or greater than 75 mm rainfall or more in one day. According to this criterion, seven events (July 22, 2016, July 2, 2017, July 9, 2017, July 10, 2017, Aug 4, 2017, Aug 12, 2017 and Aug 13, 2017) were identified during the study period which exceeds the 75mm threshold value. For this study, the satellite estimated rainfall object is denoted as forecast object. Red and green object means forecast are matched with observation object while blue object shows the unmatched between observed and forecast. Forecast objects are shown by the outlines. In this study, forecast means IMERG estimated rainfall.

#### 3.2.1 Threshold value of 150/100mm/24hr

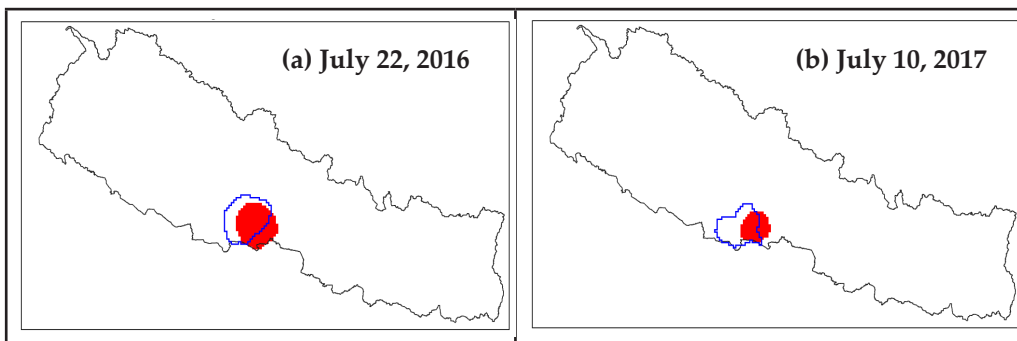
The MODE analysis of individual object and cluster for threshold value of 150/100 mm/24hr. is summarized in Figure 3. Among the seven rainfall events, MODE identified two extreme rainfall events at this particular threshold value. IMERG failed to estimate rainfall for other events taken under consideration except for July 22, 2016 and Aug 13, 2017. The total interest value is higher (0.96) for July 22, 2016 showing the better performances of IMERG for that particular event. The highest rainfall area around Hetauda region is shown by IMERG. However, the eastern and western rainfall areas are not captured by IMERG. In July 22, 2016, forecast area is greater (71grid squares) than observed area (58grid squares) means there is overestimation of areal extent of IMERG whereas in August 13, 2017, forecast area (245grid squares) is less than observed area (596grid squares) means there is underestimation of areal extent of IMERG estimated rainfall (Annex 1). Additionally, IMERG shows westward shifting of location than observation (Figure 3).



**Figure 3.** Observation object with forecast outlines for 150/100mm/24 hr. Red and green object means forecast are matched with observation object while blue object shows the unmatched between observed with forecast.

### 3.2.2 Threshold value of 100/75mm/24hr

The summary of forecast and object field compared at threshold value of 100/75mm/24hr. is shown in Figure 4 and summarized in Annex 2. In addition to events identified under 150/100 mm/24hr. threshold criteria, two new rainfall events are detected for threshold value of 100/75mm/24 hr. Altogether, four rainfall events (July 22, 2016; July 10, 2017; Aug 4, 2017 and August 13, 2017) were detected by MODE analysis. Similar results is obtained for this threshold value showing the west ward shifting of rainfall area by IMERG which is consistent with (Karki et al ., 2018), which may be due to a coarser resolution of IMERG. Also, it is evident that the number of detected pairs increases as the threshold value decreases for some of the events (Figure 4). As the total interest value measures the degree of correspondence between observed and satellite estimated precipitation pattern, this indicates that the IMERG satellite estimates is capable to reproduce some of the patterns of extreme rainfall events. Total interest value is highest (0.98) for July 22, 2016 whereas lowest (0.76) for Aug 4, 2017. The number of detected pair is higher for Aug 13, 2017. Forecast areas of three events i.e. July 22, 2016; July 10, 2017 and Aug 4, 2017 is greater than observed areas means there is overestimation of areal extent of IMERG estimation, but forecast area of Aug 13, 2017 is less than observed area means there is underestimation of areal extent of IMERG estimation.



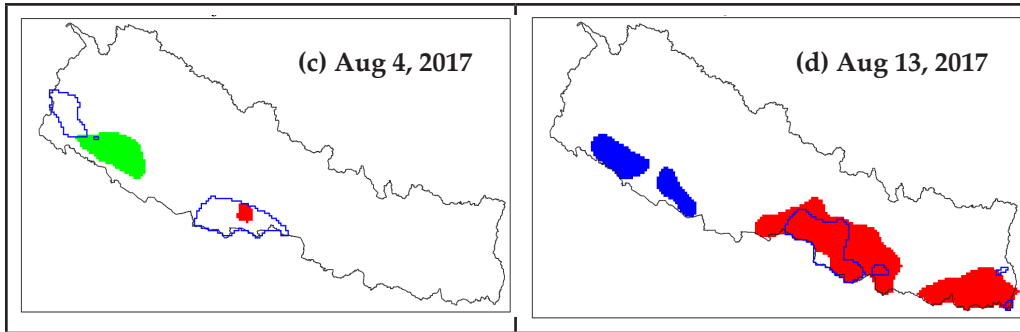


**Figure 4.** Observation object with forecast outlines for 100/50mm/24hr. Red and green object means forecast are matched with observation object while blue object shows the unmatched between observed with forecast.

### 3.2.3 Threshold value of 75/50mm/24hr.

MODE analysis of IMERG rainfall estimates and observation is also carried out for threshold value of 75/50mm/24hr (Figure 5). From the whole study period, seven rainfall events are selected for MODE analysis. Intersection area of forecast and observation area on July 2, 2017 and July 9, 2017 is zero indicating false estimates of IMERG to observation which is also verified from the low total interest value Annex 3. The total interest value for July 10, 2017 and August 4, 2017 is 1 indicates the best correspondence between satellite estimates and observation. The number of satellite estimates object is highest (6) for July 10, 2017 which is higher than observed objects (2) for same day showing the overestimation of rainfall by IMERG. Forecast area of six events i.e., July 22, 2016; July 10, 2017; July 2, 2017; July 9, 2017; August 4 2017; and August 12, 2017 is greater than observed area means there is overestimation of areal extent of SPPs, but forecast area of August 13, 2017 is lower than observed area means there is underestimation of areal extent of SPP. Westward shifting of satellite estimates is also seen for some of the events.

Taking all three thresholds in one, we see as on decreasing threshold values, the number of objects detected by satellite increases. There is underestimation of areal extent of SPP in the event of August 13, 2017 in all three threshold values. Except this event, there is an overestimation of areal extent of SPP of the other six events of heavy rainfall in all three threshold values. Centroid distance provides a quantitative sense of spatial displacement of forecast (SPP). Centroid distance is less means there is small displacement of forecast, which is good.

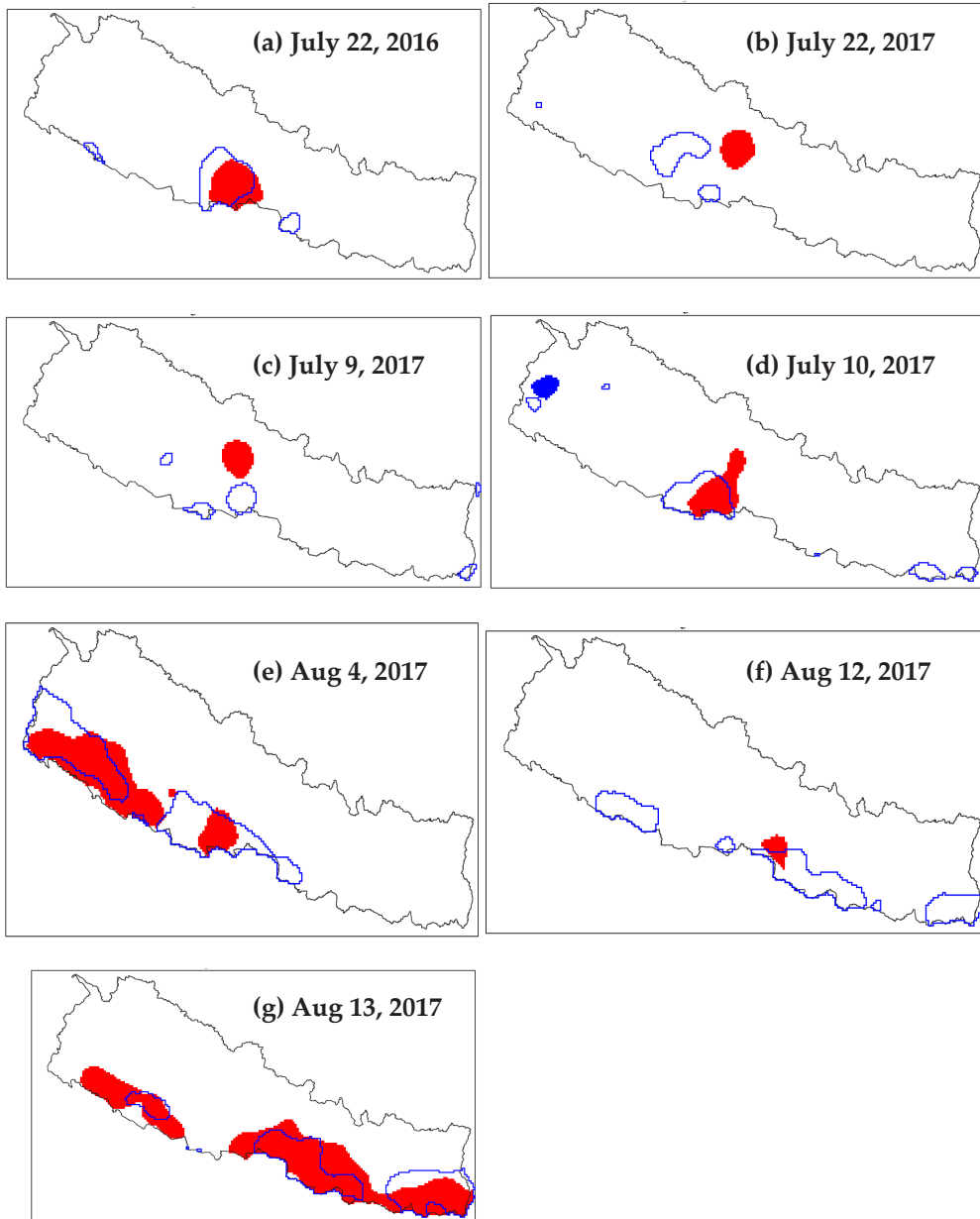


**Figure 5.** Observation object with forecast outlines for 75/50mm/24hr. Red and green object means forecast are matched with observation object while blue object shows the unmatched between observed with forecast.

## 4. Discussion

This study evaluated the performance of IMERG satellite product in detecting heavy rainfall events with reference to the observed rainfall over Nepal during the study period from Dec, 2015 to Dec, 2017. As seen from the results presented above, the performance of satellite precipitation estimates in depicting the precipitation changes over Nepal is location dependent. Consistent with this suggestion, earlier studies have also noted that the performance of IMERG in depicting precipitation changes over other regions is location dependent; (Prakash et al., 2016; Sahlou et al., 2016). For example, Gaona et al., (2016) noted that IMERG tends to underestimate the total precipitation amount over the Netherlands, while Prakash et al., (2018) noted that IMERG tends to overestimate the precipitation amount over the Arabian Sea and the Bay of Bengal.

It is identified that the spatial extent of an extreme precipitation on August 13, 2017 was east-west oriented band of maximum precipitation around the foothills of the Himalayas. It is important to mention that whole country experienced widespread distribution of rainfall during that event. Moreover, that particular event features three isolated centers located in western, central and eastern Nepal and the zone of extreme precipitation was localized in central Nepal. Record highest 24 hour accumulated rainfall of 516.2 mm was observed at Hetauda station, located in central Terai region (less than 500 m elevation) ( Figure 2). This result is consistent with Tachabhadel et al., (2020). They found one day extreme precipitation peaks are found at lower elevation (<1000m) which lies in first southern lower mountain range (Churiya range). As mentioned by Kadel et al., (2017), extreme precipitation is expected to be more severe in future on different warning scenario. Hence, the high spatial and temporal resolution of IMERG satellite product is indeed a better source of rainfall data to study extreme events over Nepal.

Compared to observed data, IMERG underestimates the 24-hour precipitation amount. IMERG estimates shows west ward shifting of extreme precipitations area which may be due to the low spatial resolution of IMERG satellite data. It agrees with the similar research done by for extreme rainfall events of August 14, 2014 over Nepal (Karki et al., 2018).

MODE analysis was done to detect the spatial location of heavy rainfall. During the study period, seven events were detected as heavy rainfall events. They were analyzed using different thresholds i.e. 150/100mm/24hr, 100/75mm/24hr and 75/50mm/24hr. In 150/100mm/24hr threshold, only two events were detected. In 100/75mm/24hr, four events were detected and in 75/50mm/24hr, seven events were detected. Also, number of objects detected by IMERG increases as threshold value decreases. In most of the heavy rainfall events, westward shifting of satellite rainfall is observed. Observation area and forecast area of all events were calculated to see either the over or under estimation of areal extent of SPPs. Among the cases in consideration for different threshold values, event of August 13, 2017 was the widespread event. SPP also indicated the same however event coverage/areal extent was underestimated by SPPs. Also, in all three cases of August 13, 2017 event, forecast area is less than observation area means there is an underestimation of areal extent of SPPs.

## 5. Conclusions

This study evaluates the recently released multi-satellite IMERG precipitation product for its accuracy to represent the extreme precipitation events using 310 DHM rain gauge observations over Nepal between December, 2015 and December 2017.

Overall, the IMERG products underestimated the observed extreme precipitation events over Nepal. We have also analyzed the extreme precipitation event occurred at Hetauda climate station on August 13, 2017 having rainfall of 516.2 mm. IMERG product well captured the heavy rainfall amount; however, it failed to capture the exact locations estimated by gauge station (with westward location shifting). Analysis using MODE tool further revealed that the IMERG estimates shows westward shifting of heavy rainfall areas in most of the events, which may be related to spatial resolution of IMERG product. Furthermore, on decreasing the threshold value of rainfall the number of detected pair of objects is increased. Moreover, this study recommends to future study need to focus on the applications of satellite rainfall products in hydrological modeling, flood forecasting and natural hazard prevention over this mountain region.

**Acknowledgements:** I would like to express my great gratitude to the DHM for providing ground-based rainfall data and NASA/Goddard Space Flight Center's Mesoscale Atmospheric Processes Laboratory and PPS, which develop and compute IMERG as a contribution to GPM, and archived at the NASA STORM PPS. I would also like to thank University Grants Commission (UGC), Nepal and UN World Food Programme (WFP), Nepal for their support.

**Conflicts of interest:** The authors declare no conflict of interest.

## References

- Chen, F., & Li, X. (2016). Evaluation of IMERG and TRMM 3B43 monthly precipitation products over mainland China. *Remote Sensing*, 8, 472. <https://doi.org/10.3390/rs8060472>
- Coning, E. (2013). Optimizing Satellite-Based Precipitation Estimation for Nowcasting of Rainfall and Flash Flood Events over the South African Domain. *Remote Sensing*, 5, 5702–5724. <https://doi.org/10.3390/rs5115702>
- Davis et al., 2009. (2009). The Method for Object-Based Diagnostic Evaluation ( MODE ) Applied to Numerical Forecasts from the 2005 NSSL / SPC Spring Program. 1252–1267. <https://doi.org/10.1175/2009WAF2222241.1>
- Disaster, D., & Governments, L. (2017). Nepal flood-2017 situation report. 4(4), 1–8.
- Gaona, M., Vereem, A., Leijnse, H., & Uijlenhoet, R. (2016). First-year evaluation of GPM rainfall over the Netherlands: IMERG day 1 final run (V03D). *Journal of Hydrometeorology*, 17. <https://doi.org/10.1175/JHM-D-16-0087.1>
- Germann, U., Galli, G., Boscacci, M., & Bolliger, M. (2007). Radar Precipitation Measurement in a Mountainous Region. *Quarterly Journal of the Royal Meteorological Society*, 132, 1669–1692. <https://doi.org/10.1256/qj.05.190>
- Hamal, K., Sharma, S., Baniya, B., Khadka, N., & Zhou, X. (2020). Inter-Annual Variability of Winter Precipitation Over Nepal Coupled With Ocean-Atmospheric Patterns During 1987-2015. *Frontiers in Earth Sciences*, 161. <https://doi.org/10.3389/feart.2020.00161>

- Hamal, K., Sharma, S., Khadka, N., Baniya, B., Ali, M., Shrestha, M. S., Xu, T., Shrestha, D., & Dawadi, B. (2020). Evaluation of MERRA-2 precipitation products using gauge observation in Nepal. *Hydrology*, 7(3), 1–21. <https://doi.org/10.3390/hydrology7030040>
- Hou, A. Y., Kakar, R. K., Neeck, S., Azarbarzin, A. A., Kummerow, C. D., Kojima, M., Oki, R., Nakamura, K., & Iguchi, T. (2014). The global precipitation measurement mission. *Bulletin of the American Meteorological Society*, 95(5), 701–722. <https://doi.org/10.1175/BAMS-D-13-00164.1>
- Huffman, G. J., Bolvin, D. T., Braithwaite, D., Hsu, K.-L., Joyce, R., Kidd, C., Nelkin, E. J., Sorooshian, S., Tan, J., & Xie, P. (2019). Algorithm Theoretical Basis Document (ATBD) Version 06 NASA Global Precipitation Measurement (GPM) Integrated Multi-satellite Retrievals for GPM (IMERG). National Aeronautics and Space Administration (NASA), March, 1–34. [https://pmm.nasa.gov/sites/default/files/document\\_files/IMERG\\_ATBD\\_V06.pdf](https://pmm.nasa.gov/sites/default/files/document_files/IMERG_ATBD_V06.pdf)
- Kadel, I., Yamazaki, T., Iwasaki, T., & Abdillah, M. (2017). Projection of future monsoon precipitation over the central Himalayas by CMIP5 models under warming scenarios. *Climate Research*, 75. <https://doi.org/10.3354/cr01497>
- Karki, R. (2018). WRF-based simulation of an extreme precipitation event over the Central Himalayas: Atmospheric mechanisms and their representation by microphysics parameterization schemes. *Atmospheric Research*, 214. <https://doi.org/10.1016/j.atmosres.2018.07.016>
- Karki, R., Hasson, S. ul, Schickhoff, U., Scholten, T., & Böhner, J. (2017). Rising Precipitation Extremes across Nepal. *Climate*, 5. <https://doi.org/10.3390/cli5010004>
- Li, Z., Yang, D., & Hong, Y. (2013). Multi-scale evaluation of high-resolution multi-sensor blended global precipitation products over the Yangtze River. *Journal of Hydrology*, 500, 157–169. <https://doi.org/10.1016/j.jhydrol.2013.07.023>
- Nayava, J. (1980). Rainfall in Nepal.
- Nepal, B., Shrestha, D., Sharma, S., Shrestha, M. S., Aryal, D., & Shrestha, N. (2021). Assessment of GPM-Era satellite products' (IMERG and GSMaP) ability to detect precipitation extremes over mountainous country nepal. *Atmosphere*, 12(2). <https://doi.org/10.3390/atmos12020254>
- Prakash, S., Kumar, R., Mathew, S., & Venkatesan, R. (2018). How accurate are satellite estimates of precipitation over the north Indian Ocean? *Theoretical and Applied Climatology*, 134, 467–475. <https://doi.org/10.1007/s00704-017-2287-2>
- Prakash, S., Mitra, A. K., Pai, D. S., & Aghakouchak, A. (2016). Advances in Water Resources From TRMM to GPM : How well can heavy rainfall be detected from space ? *Advances in Water Resources*, 88(January 1998), 1–7. <https://doi.org/10.1016/j.advwatres.2015.11.008>
- Prakash, S., Mitra, A., Pai, D., & AghaKouchak, A. (2016). From TRMM to GPM: How well can heavy rainfall be detected from space? *Advances in Water Resources*, 88, 1–7. <https://doi.org/10.1016/j.advwatres.2015.11.008>
- Qiaohong, S., Miao, C., Duan, Q., Ashouri, H., Sorooshian, S., & Hsu, K. (2017). A Review of Global Precipitation Data Sets: Data Sources, Estimation, and Intercomparisons. *Reviews of Geophysics*, 56. <https://doi.org/10.1002/2017RG000574>
- Sahlu, D., Nikolopoulos, E. I., Moges, S. A., Anagnostou, E. N., & Hailu, D. (2016). First evaluation of the day-1 IMERG over the upper blue Nile basin. *Journal of Hydrometeorology*, 17(11), 2875–2882. <https://doi.org/10.1175/JHM-D-15-0230.1>
- Sharifi, E., Steinacker, R., & Saghafian, B. (2016). Assessment of GPM-IMERG and Other Precipitation Products against Gauge Data under Different Topographic and Climatic Conditions in Iran: Preliminary Results. *Remote Sensing*, 8, 135. <https://doi.org/10.3390/rs8020135>

- Sharifi, E., Steinacker, R., & Saghafian, B. (2018). Multi time-scale evaluation of high-resolution satellite-based precipitation products over northeast of Austria. *Atmospheric Research*, 206, 46–63. <https://doi.org/10.1016/j.atmosres.2018.02.020>
- Sharma, S., Chen, Y., Zhou, X., Yang, K., Li, X., Niu, X., Hu, X., & Khadka, N. (2020a). Evaluation of GPM-Era satellite precipitation products on the southern slopes of the central Himalayas against rain gauge data. *Remote Sensing*, 12(11). <https://doi.org/10.3390/rs12111836>
- Sharma, S., Khadka, N., Hamal, K., Shrestha, D., Talchabhadel, R., & Chen, Y. (2020). How Accurately Can Satellite Products (TMPA and IMERG) Detect Precipitation Patterns, Extremities, and Drought Across the Nepalese Himalaya? *Earth and Space Science*, 7(8). <https://doi.org/10.1029/2020EA001315>
- Sunilkumar, K., Yatagai, A., & Masuda, M. (2019). Preliminary Evaluation of GPM-IMERG rainfall estimates over three distinct climate zones with APHRODITE. *Earth and Space Science*, 6. <https://doi.org/10.1029/2018EA000503>
- Talchabhadel, R., Karki, R., Thapa, B., Maharjan, M., & Parajuli, B. (2018). Spatio-temporal variability of extreme precipitation in Nepal. *International Journal of Climatology*, 38. <https://doi.org/10.1002/joc.5669>
- Tan, M. L., Ibrahim, A. L., Duan, Z., Cracknell, A., & Chaplot, V. (2015). Evaluation of Six High-Resolution Satellite and Ground-Based Precipitation Products over Malaysia. *Remote Sensing*, 7, 1504–1528. <https://doi.org/10.3390/rs70201504>
- Tang, G., Ma, Y., Long, D., Zhong, L., & Hong, Y. (2015). Evaluation of GPM Day-1 IMERG and TMPA Version-7 legacy products over Mainland China at multiple spatiotemporal scales. *Journal of Hydrology*, 533. <https://doi.org/10.1016/j.jhydrol.2015.12.008>
- Xu, R., Tian, F., Yang, L., Hu, H., Lu, H., & Hou, A. (2017). Ground validation of GPM IMERG and TRMM 3B42V7 rainfall products over southern Tibetan Plateau based on a high-density rain gauge network: Validation of GPM and TRMM Over TP. *Journal of Geophysical Research: Atmospheres*, 122. <https://doi.org/10.1002/2016JD025418>
- Adhikary, S. K., Muttill, N. and Yilmaz, A. G. 2017. *Hydrological Processes*, 31: 2143-2161.
- Karki, R., ul Hasson, S., Gerlitz, L., Talchabhadel, R., Schenk, E., Schickhoff, U., Scholten, T. and Böhner, J. 2018. *Atmospheric Research*, 214: 21-35.
- Ly, S., Charles, C. and Degré, A. 2013. *Biotechnologie, Agronomie, Société et Environnement*, 17: 392-406.
- Nepal, B., Shrestha, D., Sharma, S., Shrestha, M. S., Aryal, D. and Shrestha, N. 2021. *Atmosphere*, 12: 254.
- Soo, E. Z. X., Jaafar, W. Z. W., Lai, S. H., Othman, F., Elshafie, A., Islam, T., Srivastava, P. and Hadi, H. S. O. 2020. *Hydrology Research*, 51: 105-126.
- Sunilkumar, K., Yatagai, A. and Masuda, M. 2019. *Earth and Space Science*, 6: 1321-1335.



**Annex**

**Annex 1.MODE summary table for threshold value 150/100mm/24hr.**

S.N	Event	Centroid Distance	Forecast Area	Observation Area	Intersection Area	Union Area	Total Interest	POD	FAR	Accuracy	No of obj	
											Sat	Obs
1	July 22,2016	4.62	71	58	22	107		0.96	0.99	0.99	0.01	1
2	July 2,2017	-	-	-	-	-		-	-	-	-	-
3	July 9,2017	-	-	-	-	-		-	-	-	-	-
4	July 10,2017	-	-	-	-	-		-	-	-	-	-
5	Aug 4,2017	-	-	-	-	-		-	-	-	-	-
6	Aug 12,2017	-	-	-	-	-		-	-	-	-	-
7	Aug 13,2017	10.55	245	596	128	713		0.94	0.89	0.99	0.11	1

**Annex 2.MODE summary table for threshold value 100/75mm/24hr**

S.N	Event	Centroid Distance	Forecast Area	Observation Area	Intersection Area	Union Area	Total Interest	POD	FAR	Accuracy	No of obj	
											Sat	Obs
1	July 22,2016	5.06	281	247	163	365		0.98	0.99	0.03	1	1
2	July 2,2017	-	-	-	-	-		-	-	-	-	-
3	July 9,2017	-	-	-	-	-		-	-	-	-	-
4	July 10,2017	6.67	219	122	78	263		0.98	0.99	0.01	1	1
5	Aug 4,2017	4.34	393	42	42	393		0.91	0.94	0.04	3	2
		25.29	186	335	6	515		0.76				
6	Aug 12,2017	-	-	-	-	-		-	-	-	-	-
7	Aug 13,2017	17.52	492	1,504	453	1,543		0.91	0.94	0.04	4	4

Annex 3.MODE summary table for threshold value 75/50mm/24hr

S.N	Event	Centroid Distance	Forecast Area	Observation Area	Intersection Area	Union Area	Total Interest	POD	FAR	Accuracy	No of obj	
											Sat	Obs
1	July 22_2016	35.92	733	87	32	788	0.87	0.90	0.91	0.01	3	1
2	July 2_2017	23.12	319	192	0	511	0.69	0.95	0.97	0.02	3	1
3	July 9_2017	19.84	186	181	0	367	0.72	0.96	0.98	0.02	5	1
4	July 10_2017	8.73	415	360	228	547	1.00	0.94	0.97	0.05	6	2
5	Aug 4_2017	9.03	1,526	1,172	729	1,969	1.00	0.87	0.91	0.12	3	3
6	Aug 12_2017	35.92	733	87	32	788	0.87	0.90	0.91	0.01	5	1
7	Aug 13_2017	24.69	1,556	2,370	1,288	2,638	0.97	0.86	0.96	0.24	5	2